THE JOURNAL OF PHYSICAL CHEMISTRY C

Article

Cite This: J. Phys. Chem. C 2019, 123, 17598−17605

pubs.acs.org/JPCC

Conformational Changes of Protein upon Encapsulation of Noble Metal Clusters: An Investigation by Hydrogen/Deuterium Exchange Mass Spectrometry

Debasmita Ghosh,[†] Sathish Kumar Mudedla,[‡] Md Rabiul Islam,[†] Venkatesan Subramanian,[‡] and Thalappil Pradeep*[,†]

[†]DST Unit of Nanoscience (DST UNS) & Thematic Unit of Excellence (TUE), Department of Chemistry, Indian Institute of Technology Madras, Chennai 600036, India

[‡]Chemical Laboratory, CSIR-Central Leather Research Institute, Adyar, Chennai 600020, India

Supporting Information

ABSTRACT: Hydrogen/deuterium exchange mass spectrometry was employed to probe the conformational changes in lysozyme (Lyz) during the course of formation of a protein-protected atomically precise Au_8 cluster. MALDI MS showed the protein, Lyz, to be present in a denatured state in the cluster. Detailed ESI MS analysis of the Au-attached Lyz adducts, an intermediate of cluster formation, confirmed that these conformational changes are brought about by Au−S bond formation and a similar conformation is retained in the final cluster. These results were supported by computational results, which showed an increase in solvent accessible surface area upon the formation of the adducts. Infrared spectroscopy established that change in the rate as well as the extent of the hydrogen/deuterium exchange observed in the cluster was due to the change in the amide II region of the encapsulating protein. Hydrogen/deuterium exchange ESI MS of Cu adducts of Lyz showed a lower degree of denaturation than their Au counterparts. XPS analysis revealed that Cu binds differently to Lyz than it does with Au, which is likely because of the stronger soft−soft Au−S interaction. Alkali metal ion binding, on the other hand, does not affect the protein conformation because such ions do not affect the disulfide bonds.

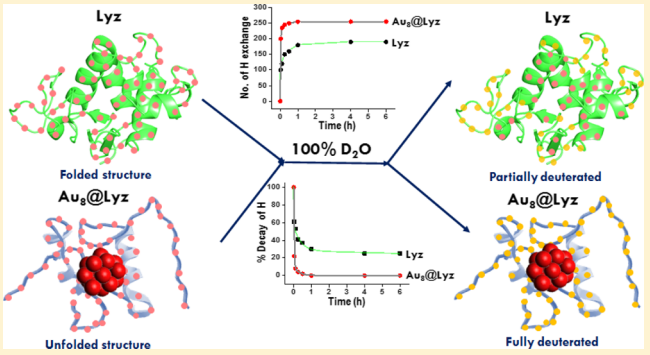

INTRODUCTION

Protein-protected clusters[1,2] have been found to be useful as chemical sensors[3−5] due to their excellent inherent photoluminescence, which is easily affected by the presence of foreign bodies in the medium. Their ease of synthesis, exceptional stability, and biocompatibility have also resulted in applications in imaging,[6] drug delivery,[7] and other biomedical fields.[8] Despite their wide range of applications, very little is known about the structure of protein-protected clusters. This is in stark contrast to their monolayer-protected counterparts, the exact atomic structure for several of those have been derived successfully.[9−11] Understanding the structure of these clusters can not only help shed light on their unique reactivity[12−14] but also help tune their luminescence[15] and surface functionality.[16] A similar clear understanding of the structure of protein-protected clusters will help fine tune these clusters for specific problems, pushing the envelope of their applications to the next level.

Protein-protected clusters are biohybrid materials, in which an inorganic cluster composed of tens of atoms of noble metals is grown inside a protein template. The complete structural identification of a protein-protected cluster would thus require characterization of both these components. Structure of the proteins is generally derived from X-ray crystallography[17,18] or single-particle cryoelectron microscopy.[19,20] X-ray crystallography is one of the main techniques used for the characterization of monolayer-protected clusters as well.[21] However, protein-protected clusters could not be crystallized till date, and thus X-ray structure could not be determined. MALDI MS has been used traditionally to characterize such clusters. Detailed understanding of the growth kinetics of gold clusters in proteins through comprehensive MALDI MS analysis of the intermediates was published in an earlier work.[22] However, such traditional mass spectrometric analysis could only reveal the atomicity of the clusters formed and not their structure. Synchrotron-based X-ray absorption fine structure spectroscopy was used more recently to identify the core structure, and interlocked gold−thiolate rings were identified, departure from the monolayer-protected ones which generally consist of a metal core protected by metal thiolate motifs.[23] However, the

Received: April 29, 2019
Revised: June 12, 2019
Published: June 25, 2019

DOI: 10.1021/acs.jpcc.9b04009
J. Phys. Chem. C 2019, 123, 17598−17605

aspicule structure of monolayer-protected clusters had suggested the existence of gold−thiolate rings in them.

Structural alteration of the protecting proteins in these clusters has not been examined well so far. This is an extremely important aspect to be addressed because the structure of a protein is closely related to its biological function. Any undesired alteration of the structure of its active site thus might lead to complete loss of such functions in the formed clusters. The cluster formation has been shown to increase the overall hydrodynamic diameter, indicating a departure from the native state of the corresponding protein.[24] It is known that Au−S bond formation is associated with breakage of the disulfide bonds in the protein and is likely to bring about structural changes. In our earlier work, by combining ion mobility with electrospray ionization (ESI) mass spectrometry, we showed that successive attachment of Au atoms to the protein backbone leads to gradual unfolding of the protein.[25] However, whether such unfolded conformers of the protein end up being retained in the final cluster or not was not addressed.

In the following, we present an investigation into the conformational change of lysozyme (Lyz) from its native state to the final cluster by hydrogen/deuterium exchange mass spectrometry and infrared spectroscopy. The extent of change in protein-protected clusters was found to be similar to that of the Au-attached protein adducts, implying that structural changes arise right from the initial stage of metal binding itself. Fast exchange of all labile hydrogens in the amide backbone of the adducts confirmed their greater solvent accessibility compared to the protein, courtesy of their unfolded nature. Similar unfolded structure of the protein leads to a rapid and complete exchange of all hydrogens in the cluster. This study has given a new insight into the changes in the protein structure upon cluster formation, which has been difficult to explore. The extent of structural change in Lyz was observed to be more for Au binding than for Cu and alkali-metal ions. Computations allowed us to understand the change in the solvent accessible area of protein and the specific regions in which such changes occurred. Collectively, data present new insights into an unknown area of structural changes in a protein in protein-protected clusters.

METHODS

Materials. Tetrachloroauric acid trihydrate ($HAuCl_4 \cdot 3H_2O$) was prepared in-house starting from elemental gold. Lyz (>90% purity) was purchased from Sigma-Aldrich. Sodium hydroxide pellets were purchased from a local supplier (Rankem, India). Milli-Q water and D_2O (Sigma-Aldrich) were used in all experiments. Sinapic acid (99% purity) used as a matrix for MALDI MS was purchased from Sigma-Aldrich. All chemicals in the experiment were used without further purification.

Instrumentation. Most of the experiments reported in this paper were carried out using a Waters Synapt G2Si HDMS instrument. This instrument consists of an electrospray source, quadrupole ion guide/trap, ion mobility cell, and TOF detector. Different gases were used in different parts of the instrument. All experiments were carried out in the positive ion mode. NaI was used for the calibration of the instrument. To get a well-resolved mass spectrum, the following optimized conditions were used.

Sample concentration: 1 μg/mL.
Solvent: water and D_2O.
Flow rate: 10−20 μL/min.
Capillary voltage: 2−3 kV.
Cone voltage: 20 V.
Source offset: 20 V.
Desolvation gas flow: 400 L/h.
Source temperature: 100 °C.
Desolvation temperature: 150 °C.

Fourier transform infrared (FTIR) spectra were measured with PerkinElmer Spectrum 2 with UATR attachment.

MALDI MS data of Lyz and Au_8@Lyz cluster were measured using a Voyager-DE PRO Biospectrometry Workstation of Applied Biosystems. A pulsed nitrogen laser of 337 nm was used for ionizing the protein and the cluster in the presence of the sinapic acid matrix. Spectra were collected in the positive mode and an average of 250 shots was used for each spectrum. The matrix solution was prepared using 1:3 mixture of acetonitrile and 0.1% trifluoroacetic acid (TFA) in Milli-Q water. For 100% D_2O experiment, acetonitrile-d_3, deuterated TFA, and D_2O was used in the same ratio. The cluster solution (5 μL) was mixed thoroughly with 50 μL of the matrix mixture. The resulting mixture (2.5 μL) was spotted, and the dried droplet was used for analysis.

Synthesis of Au_8@Lyz. Lyz (5 mg) was dissolved in 1 mL of Milli-Q water. 1.25 mM Au^{3+} aqueous solution was incubated with Lyz to make Au_n−Lyz adducts. NaOH (1 M) (100 μL) was added to the adduct to make Au_8@Lyz clusters. Before ESI MS, the adducts were diluted in Milli-Q water. For the hydrogen/deuterium exchange study, the samples were diluted in H_2O as well as D_2O. Finally, for a 100% hydrogen/deuterium MS experiment, the Au_n−Lyz adduct and the cluster was lyophilized and then dissolved in 100% D_2O.

Computational Details. In our previous study, gold-induced structural changes in Lyz were investigated using classical molecular dynamics simulations.[25] The simulated structures from our previous study have been taken further to understand the dynamics for 150 ns. In the simulations of Lyz and Au_8−Lyz, similar protocols were followed as in our previous study. The structure of Lyz was taken from the protein data bank (pdb id: 1AKI).[17] Details of the secondary structure have been calculated using dictionary of the secondary structure of the protein protocol.

RESULTS AND DISCUSSION

Brown-colored Au_8@Lyz cluster solution exhibits intense red luminescence under UV light irradiation (inset, Figure 1a). The UV−vis spectrum of this cluster solution showed one broad peak around 280 nm and a broad hump from 320 to 380 nm, shown in Figure S1. This luminescent cluster showed two broad excitation peaks, one between 340 and 380 nm and another between 450 and 550 nm along with two emission peaks at 440 and 650 nm (Figure 1a). The first peak corresponds to the protein shell and the second one is due to the cluster core, respectively. Two-step formation of Au_8@Lyz involving the addition of Au^{3+} ions to form the Au_n−Lyz complex in the first step is followed by the addition of NaOH to complete the cluster formation inside the protein moiety in the second step, and it is shown schematically in Figure 1b.

The luminescent cluster along with its parent protein (Lyz) was subjected to MALDI MS to probe the atomicity of the gold core. Lyz showed its molecular ion peak at 14.3 kDa and a shift of 1576 Da from the parent protein confirmed the formation of the Au_8 core inside the Lyz cavity (Figure 1c). Lyz consists of a total of 129 amino acids, 19 basic groups, and 255 labile hydrogens with 126 amide groups in the backbone.[26]

DOI: 10.1021/acs.jpcc.9b04009
J. Phys. Chem. C 2019, 123, 17598−17605

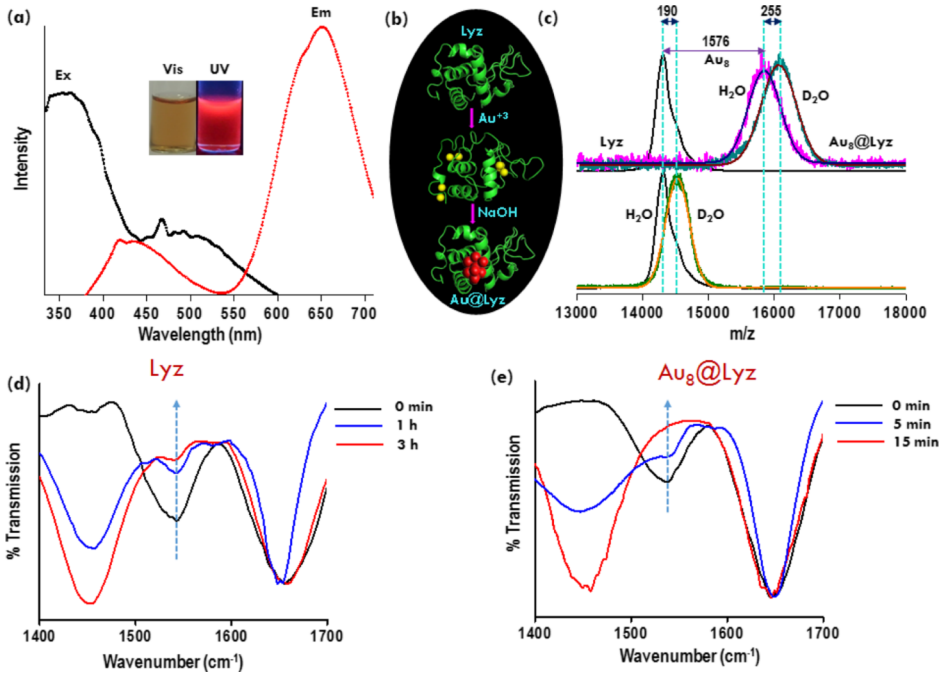

Figure 1. (a) Excitation and emission spectra of the Au_8@Lyz cluster. Photographs of the cluster solution taken under visible and UV light are shown in the inset. (b) Schematic representation of the one-pot formation of the luminescent cluster. (c) MALDI MS of Lyz (lower panel) and Au_8@Lyz (upper panel) showing their H/D exchange behavior. Time-dependent H/D exchange IR spectra for Lyz (d) and Au_8@Lyz (e). Time refers to the time of exchange reaction.

To access the change in the conformation of Lyz during the course of cluster formation, hydrogen/deuterium exchange mass spectrometry was employed. In these experiments, both Lyz and Au_8@Lyz were allowed to exchange for 24 h in 100% D_2O, followed by MALDI MS to quantify the number of exchanges in both the cases. The deuterated matrix was used in MALDI MS sample preparation to avoid the possibility of back exchanges. A shift of m/z 255 was observed in the spectrum of Au_8@Lyz, corresponding to the exchange of all the labile hydrogens associated with the amide backbone but a shift of only m/z 190 was observed for Lyz (Figure 1c). It indicates that all amide hydrogens were exchanged in the clusters, unlike in the case of the protein. It is to be noted that continuing the hydrogen/deuterium exchange reaction beyond 24 h for Lyz did not increase the extent of exchange, shown in Figure S2. The exchange behavior exhibited by Au_8@Lyz was very similar to that of denatured Lyz, reported earlier.[26] Denaturation of Lyz using dithiothreitol results in the breakage of the disulfide bonds, making all the amide hydrogens available for exchange; some of them are not available in the original globular form. Interaction of Au^{3+} with Lyz in the first step of cluster formation also results in the cleavage of disulfide bonds and formation of Au−S bonds.[27] Consequently, all amide hydrogens of Au_8@Lyz get exposed to the solvent, indicating structural alteration of Lyz upon cluster formation.

Monitoring the hydrogen/deuterium exchange with IR spectroscopy for both Lyz and Au_8@Lyz provided strong support to the mass spectrometric observations. The solutions of native Lyz and freeze-dried Au_8@Lyz in pure D_2O were subjected to time-dependent IR spectroscopy, and the intensity of the amide II band was closely monitored. In the deuterated medium, the band which originally appears around 1550 cm^{-1} (band II) got shifted to around 1450 cm^{-1}. The hydrogen/deuterium exchange (Figure 1d) resulted in a gradual decrease in the intensity of band II along with an increase in the intensity of 1450 cm^{-1}. However, it is important to note that complete disappearance of band II was never observed, even after prolonged (24 h) incubation. On the other hand, the complete disappearance of band II happened within 15 min in the case of Au_8@Lyz (Figure 1e). Note that spectra were collected with attenuated total reflection−FTIR and data collection typically took <1 min. This shows a clear difference in the secondary structure between Lyz and the protein shell in Au_8@Lyz. A similar observation of the hydrogen/deuterium exchange was reported for heated protein solutions where heat promotes the formation of random coils.[28] Hydrogen/deuterium exchange of heated Lyz is shown in Figure S3. The random coils formed were exposed more to the solvent compared to highly organized α-helixes and β-sheets. Therefore, complete hydrogen/deuterium exchange happened, at a faster rate. During cluster formation, the protein secondary structure gets similarly uncoiled; thus, complete exchange is observed in the case of Au_8@Lyz, unlike in the native protein.

Further insights into the rate of the hydrogen/deuterium exchange in connection with change in the protein conformation during cluster formation required a fast analysis method with minimal sample preparation to perform time-dependent analysis. Because MALDI MS requires extensive sample preparation, it is unsuitable for such a study. ESI, on the other hand, is a fast soft ionization method, which produces intact, multiple protonated ions from protein molecules in solution without the need of sample preparation.[26] Moreover, the well-defined charge state distribution of a protein in ESI MS is often used as a thumbprint and change in their charge state distribution is used to probe the changes in protein conformations, making it a suitable technique for our purpose. The conformational alteration of the protein due to the formation of Au_n−Lyz adducts in the first step of cluster formation was probed first to get an idea about the changes associated with the breakage of the disulfide bonds in this step.

DOI: 10.1021/acs.jpcc.9b04009
J. Phys. Chem. C 2019, 123, 17598−17605

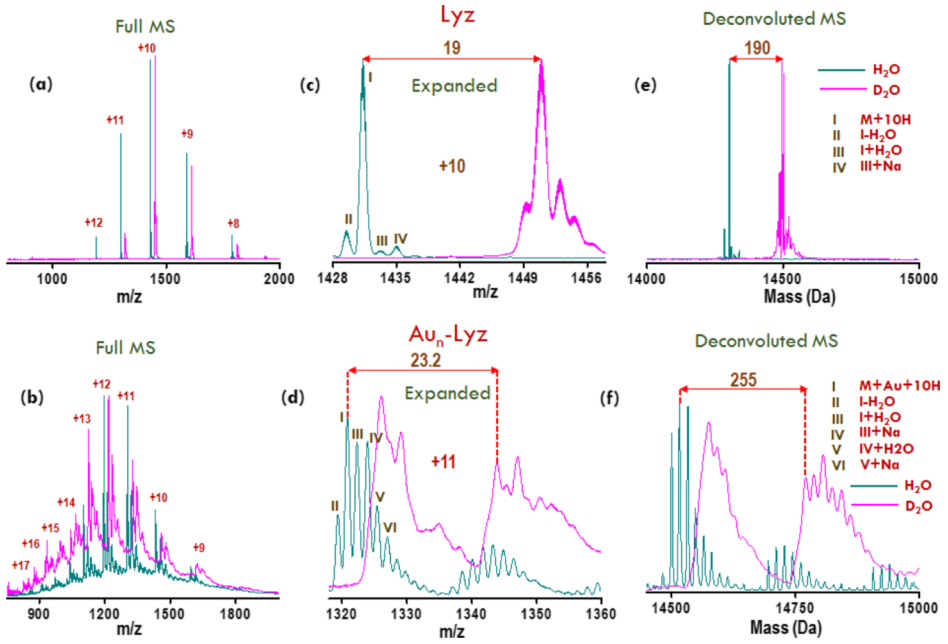

Figure 2. H/D exchange mass spectra of Lyz and Au_n−Lyz, respectively, in 100% D_2O, ESI MS (a,b); expanded ESI MS from a single-charge state (c,d); and deconvoluted MS (e,f).

The net positive charge on the native protein in solution is lower than the unfolded one. Protein molecules are tightly folded in their native state having some of their basic sites buried and involved in strong H-bonded interaction, and these do not protonate in solution.[26] This is observed in ESI MS of Lyz (Figure 2a), which consists of 129 amino acid residues having 19 basic sites, but all these charge states do not appear in the mass spectrum. Interaction of Lyz with Au^{3+} during cluster formation results in the breakage of all four disulfide bonds present in it. This in turn unfolds the protein, and all basic sites became exposed to the solvent, resulting in an increment in the intensity of the higher charge states (Figure 2b). The simulated structures of Lyz and Au_8−Lyz were shown in Figure S4. The loss of the helical content on binding with gold ions was noticed when compared to parent Lyz. Helical and beta conformations after binding of gold ions decreased by 15 and 3%, respectively. A decrease in the number of H-bonds between the backbones, which is responsible for the formation of different secondary structures, was calculated (Figure S5). The reduction of hydrogen bonds is more in the case of Au_8−Lyz than for Lyz. The average number of hydrogen bonds in Lyz and Au_8−Lyz are 88 and 76, respectively. The reduction of hydrogen bonds correlates with the loss of helical and beta sheet content due to adduct formation, in line with the denaturation of Lyz in the process. Spectra obtained after a complete exchange of replaceable hydrogens for both Lyz and Au_n−Lyz in 100% D_2O are overlaid in Figure 2a,b, respectively. Expansion of the +10 charge state for Lyz and +11 charge state for Au_n−Lyz (selected due to reduction in the intensity of the +10 state), respectively, is shown in Figure 2c,d, which showed clear differences in deuterium exchange that became apparent upon deconvolution. The deconvoluted spectrum for Lyz (Figure 2e) showed a mass shift of 190; same was observed in MALDI MS, while Au_n−Lyz (Figure 2f) showed a mass shift of 255. The mass shift for Au_n−Lyz adducts matched with the mass shift observed for the Au_8@Lyz clusters. This points to the fact that structural change in the amide region of the protein happens in the beginning stage of incubation with Au^{3+} ions, and the cluster acquires a similar protein shell structure, in terms of position and accessibility of the amide groups. Because the final cluster (Au_8@Lyz) does not ionize under electrospray conditions, detailed experiments were carried out with the Au_n−Lyz adducts.

A basic idea about the extent of structural change in the proteins could be derived by exploring how fast and how many of the hydrogens can be exchanged.[29] This again would be dependent on both the exposure of exchangeable hydrogens toward the solvent molecules as well as the percentage of D_2O in the surrounding medium. To account for both these effects, we monitored the kinetics of exchange at different D_2O concentrations (20, 50, and 100%) through ESI MS. Surprisingly, at the lowest D_2O (20%) concentration, both Lyz and Au_n−Lyz exhibited similar behavior in terms of speed of exchange and the number of total hydrogens exchanged (Figure S6). This indicates that parts of the protein structure remained intact even after cluster formation. Because the structure is closely related to protein function, those functional parts are also likely to remain intact, which has been seen in the past.[30] We have not evaluated the functions of Au_8@Lyz. Increasing the D_2O concentration to 50% starts to show differences in the exchange behavior. Figure 3a shows the hydrogen/deuterium exchange of the native protein with time, and Figure 3b shows the same for the Au-added protein. Time-dependent exchange shows gradual change in the case of Lyz, which is distinct from the adduct behavior. Figure 3c,d shows the exchange behavior for the native protein and Au-added protein in 100% D_2O, respectively. In 50% D_2O, a shift in the m/z value is less for both of the species. This can be explained in two ways. One aspect is that as the samples are in equilibrium, the back exchange made a broad distribution. The other possibility is that reduced availability of deuterium in 50% than in 100% medium made the difference. In 100% medium, the environment is fully deuterated, and there was no back-exchange, thus the difference for both the species will increase. In the case of the adduct in 100% D_2O, within 15 min, all exchangeable hydrogens were exchanged with

DOI: 10.1021/acs.jpcc.9b04009
J. Phys. Chem. C 2019, 123, 17598−17605

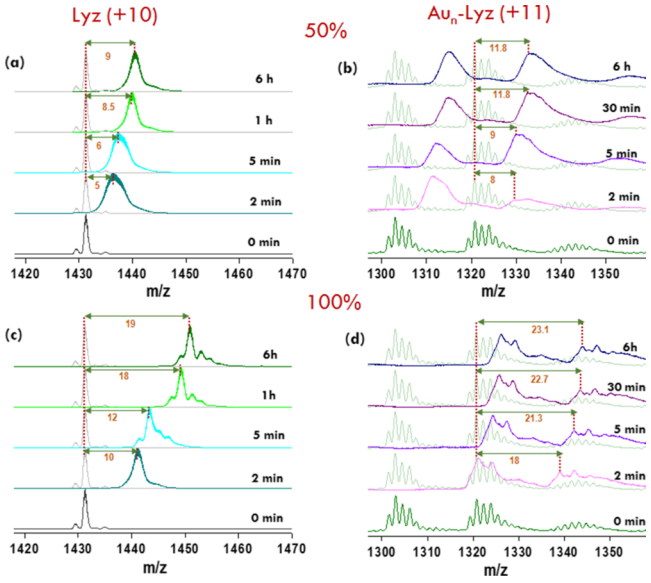

Figure 3. Time-dependent MS of Lyz and Au$_n$−Lyz in 50 and 100% D_2O in specific regions. (a,c) Change of the mass spectrum for Lyz with time in 50 and 100% D_2O, respectively, (b,d) same data for Au$_n$−Lyz. The MS of Lyz and Au$_n$−Lyz are in +10 and +11 charge states, respectively.

deuterium, whereas for the parent protein, 180 hydrogens were exchanged in 1 h. This large change in the number and the time of hydrogen exchange of the adduct points toward the structural change of the adduct. Addition of Au^{3+} to Lyz increased the availability of the amide hydrogens for exchange. The ESI MS of hydrogen/deuterium exchange (with all the charge states) in 50% D_2O (Figure S7) and in 100% D_2O (Figure S8) are presented separately.

A kinetic plot of the % decay of H, that is, reduction in number of hydrogen due to exchange with deuterium and total number of H exchanged with time is presented in Figure 4a. When a protein is exposed to D_2O environment, the rate of hydrogen exchange will depend on the presence of the amide hydrogens whether they are H-bonded or accessible to the aqueous solvent. The kinetics of percentage decay of hydrogen with time is fitted for both the species. Because a mono- and biexponential fit was inadequate to cover all the data points, a triexponential fit was used. The three rate constants, k_1, k_2, and k_3 are 0.7×10^2 h^{-1}, 0.2×10 h^{-1}, and 0.2×10^{-1} h^{-1} for native protein and for the adduct, the values are, respectively, 16×10^2 h^{-1}, 3.3×10 h^{-1}, and 33×10^{-1} h^{-1}. Initially, the exchange rates were fast but with time, it decreased. The difference in the rate constants indicates the difference in the structure of the exchanging species. This difference indicates that the amide hydrogens in the adduct were more exposed to the solvent than the protein. Solvent accessible surface area (SASA) is the surface area of a biomolecule, which is accessible to smaller molecules.[31] The calculation of SASA is often used to determine the folding and stability of the protein in solution. The calculation of the SASA value at the atomic level is very difficult experimentally. The breakage of hydrogen bonds between amide bonds in the helical conformation made the hidden back bone expose to the environment. Figure 4b showed that the calculated SASA value was more for the adduct than for the native protein. The overlapped structure (amide region) of the adduct and Lyz (Figure 4c) and the same in mapped surface areas (Figure S9) showed the increased surface area in Au$_8$−Lyz compared to Lyz. The availability of amide bonds to the environment increased the hydrogen/deuterium exchange, which was observed in our experiments. The increased value in the adduct indicated the unfolded structure of the protein. During cluster formation, the folded structure of Lyz became relaxed and less ordered. This change in the protein structure enhanced the exchange rate than the tightly folded structure of native Lyz.

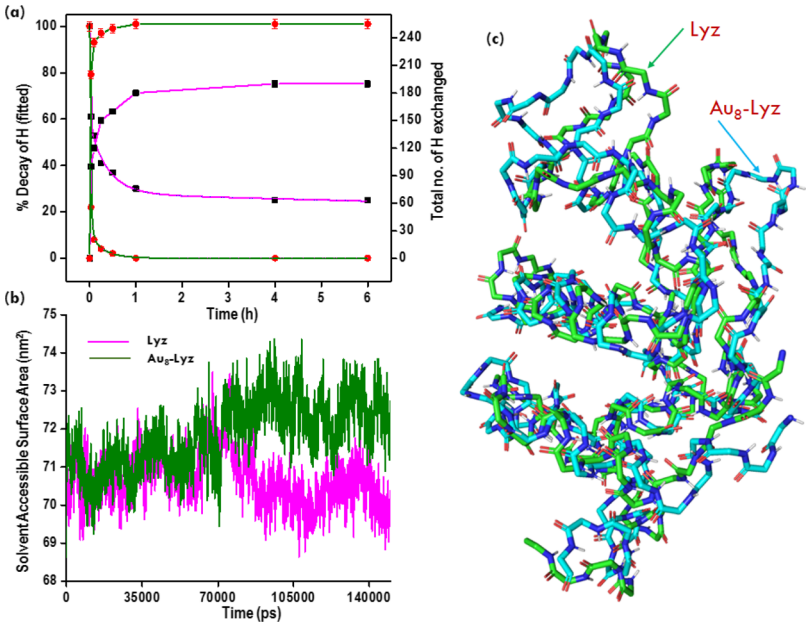

Figure 4. (a) Comparison of H/D exchange kinetics of Lyz and Au$_n$−Lyz in 100% of D_2O. The % decay in the number of H and total number of H exchanged is plotted against reaction time. The decay curve was fitted triexponentially. (b) Computationally obtained SASA for Lyz and Au$_n$−Lyz. (c) Overlapped structures of Lyz and the protein backbone (without the metal) of Au$_8$−Lyz, showing structural deviation from the native state.

DOI: 10.1021/acs.jpcc.9b04009
J. Phys. Chem. C 2019, 123, 17598−17605

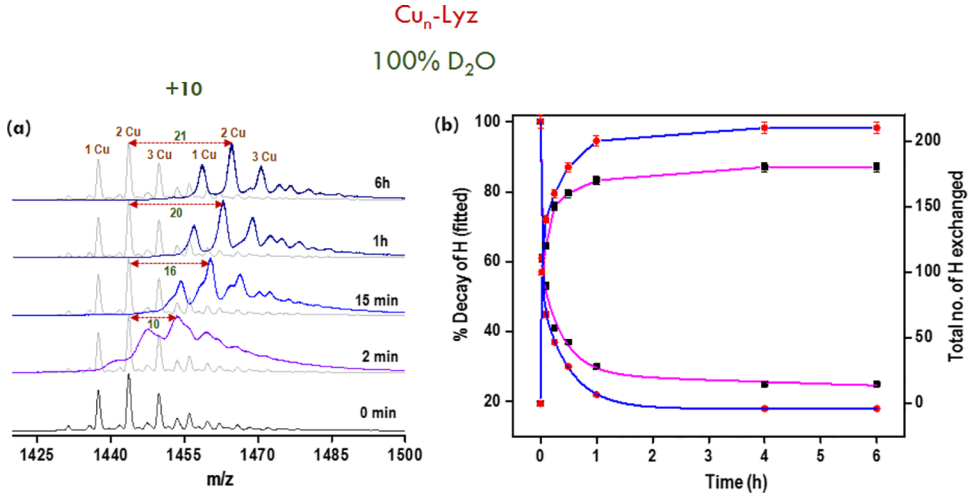

Figure 5. (a) Time-dependent MS of Cu$_n$−Lyz in 100% D$_2$O, showing the changes in the +10 charge state. (b) % decay of H and total number of H exchanged with time. The decay curve was fitted with a triexponential function.

Although not as diverse in their applications as the Au ones, protein-protected Cu clusters have also been synthesized. These clusters are generally blue luminescent,[32,33] though a few red luminescent ones have also been reported.[34] Cu^{2+} salts are generally used as the precursor to synthesize such clusters. To explore if metal to protein interaction follows a general trend leading to the formation of clusters, we prepared Cu$_n$−Lyz adducts and followed their hydrogen/deuterium exchange behavior. ESI MS of Cu$_n$−Lyz adducts showed that a maximum of eight Cu could bind with Lyz (Figure S10).[35] The time evolution of hydrogen/deuterium exchange, followed with ESI MS, for the +10 region (Figure 5a), in 100% D$_2$O medium showed a few key differences than in Au$_n$−Lyz adducts. While the total number of hydrogens exchanged were higher than that in Lyz (Figure 5b), the rate of exchange was much slower than in Au$_n$−Lyz. A similar observation was again made when the reaction was performed in 50% D$_2$O medium (Figure S11). Moreover, a complete exchange of all exchangeable hydrogens was never achieved in these cases, even with prolonged incubation of Cu$_n$−Lyz in 100% D$_2$O (data are presented in Figures S12 and 5a). To compare the kinetics, the rate constants of hydrogen/deuterium exchange were calculated in 100% D$_2$O environment (Figure 5b). Slightly higher values of the rate constant were observed for Cu$_n$−Lyz (k_1, k_2, and k_3 were 0.7×10^2 h^{-1}, 0.4×10 h^{-1}, and 0.5×10^{-1} h^{-1}, respectively), albeit of the same order as observed in Lyz. This indicates that while Cu-binding also alters the structure of a protein from its native state, the degree of alteration is less pronounced than brought about by Au binding. This could possibly stem from differences in the mode of binding of the metal ions.

XPS of both Au$_n$−Lyz and Cu$_n$−Lyz was performed to confirm whether different binding modes of metal ions are indeed responsible for the different degrees of alteration of the protein structure. The XPS spectrum in the Au 4f region (Figure 6a) showed that almost all gold is in the +1 charge state (Au $4f_{7/2}$ and Au $4f_{5/2}$ at 85.2 and 88.9 eV, respectively). This is in line with the notion that Au^{3+} oxidizes and breaks the disulfide bonds in protein and gets reduced to Au^{1+} in the process (during the first step of cluster synthesis). XPS of Au 4f for the cluster is shown in Figure S13. Cu $2p_{3/2}$ in Cu$_n$−Lyz was observed at 940.4 eV (Figure 6b), revealing that copper

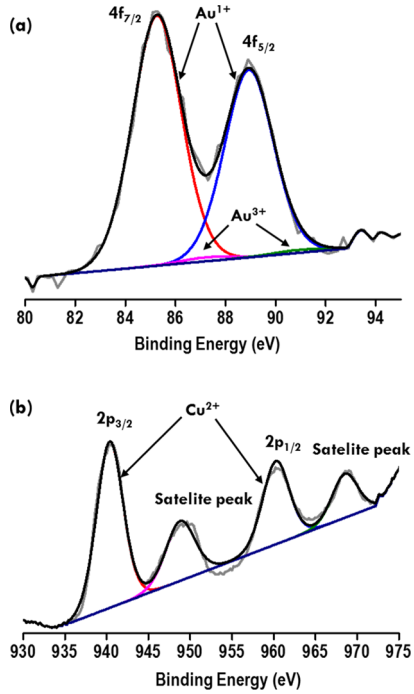

Figure 6. XPS spectra of Au$_n$−Lyz (a) and Cu$_n$−Lyz (b), in the Au 4f and Cu 2p regions, respectively, showing that Au^{1+} and Cu^{2+} are present in them. Peaks were fitted after background subtraction.

remained in the +2 oxidation state in the adduct. The configuration interaction satellite peaks for both Cu $2p_{3/2}$ and $2p_{1/2}$ were also present. The presence of Cu^{2+} in the Cu$_n$−Lyz adduct indicates that its binding to Lyz does not involve oxidation−reduction reaction unlike in the case of Au. It is likely that Cu binding does not result in complete disruption of the disulfide bonds, and hence, the protein structure was found to be less altered. A higher degree of affinity of S toward Au over Cu could very well be the reason for their different binding modes in proteins.

ESI MS examination of the alkali metal adducts of Lyz showed clear differences in their interaction in comparison to Au and Cu. Attachment of 8−10 Na^+ ions, 6−8 K^+ ions, and 2−3 Rb^+ ions is shown in Figure 7a. With increase in the ionic

DOI: 10.1021/acs.jpcc.9b04009
J. Phys. Chem. C 2019, 123, 17598−17605

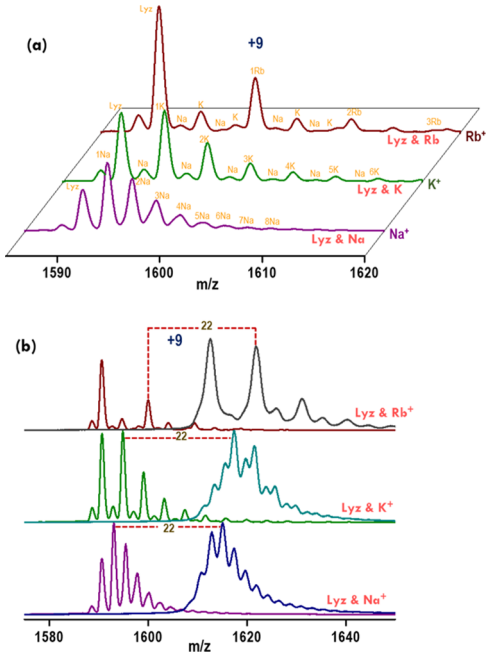

Figure 7. Interaction of Lyz with alkali metals; (a) ESI MS of alkali metal-attached Lyz adducts. (b) H/D exchange MS in the +9 charge state of alkali metal−Lyz adducts in 100% D_2O showing similar exchange for all alkali metal ions.

radii down the group showed reduced number of attachments. However, a very similar distribution of the charge state to native Lyz for all alkali metal ions (Figure S14) confirms retention of the protein structure in these adducts. The interaction of alkali metals with protein is of great interest due to their physiological roles and has been studied extensively. They are known to coordinate with proteins through cation−pi interactions. Aromatic amino acids of proteins such as phenylalanine, tyrosine, and tryptophan are the binding sites for such interaction.[36] Na^+ has been known to bind with indole present in the side chain of tryptophan residues in the case of Lyz.[37,38] Hydrogen/deuterium exchange MS studies further prove the retention of protein conformation upon alkali metal ion binding (Figure 7b). The number of hydrogens exchanged was the same for all these ions and are also equal to that for Lyz. Because for the aromatic amino acids, which are the binding sites for alkali metal ions remaining exposed to the solvent in the native protein itself, the metal ion attachment does not affect the structure of the protein. On the other hand, both Au and Cu binding affect the disulfide bonds in Lyz, bringing about large structural changes in the process.

CONCLUSIONS

Conformational changes in the protein structure in the Au_8@Lyz cluster were manifested in more protons being exchanged in hydrogen/deuterium exchange mass spectrometry. The uncoiling of Lyz during the course of cluster synthesis exposes all 255 amide hydrogens to the solvent, making their exchange possible. A part of these amide groups remain buried deep inside, in the tightly folded native state of Lyz, resulting in only 190 exchanges. These changes in the amide region of the protein became further apparent from IR spectroscopy. Mass spectrometric examination of the intermediate Au-bound Lyz adducts revealed their uncoiled nature to be similar to Au_8@Lyz and was supported by the computational results. Attachment of Au^{3+} ions to the cysteine residues through the cleavage of the disulfide bonds in the first step of cluster synthesis brings about structural changes in Lyz and those are retained in the final cluster. Structural deviation in the Cu_n−Lyz complexes was much less prominent than the Au ones, while alkali metal ions did not alter the structure at all. This could be attributed to the lower binding affinity of Cu toward S than Au and therefore, the corresponding ions interact differently with Lyz. For alkali metal ions, binding occurs only on the exposed amino acids. This study presents a step toward understanding the structure of the protein shell in protein-protected clusters, without which a complete picture of these complex entities would remain elusive.

ASSOCIATED CONTENT

Supporting Information

The Supporting Information is available free of charge on the ACS Publications website at DOI: 10.1021/acs.jpcc.9b04009.

IR spectra of heat-treated Lyz in D_2O, simulated structure of Lyz and Au_8−Lyz, simulated data for breaking of H-bonds in Au_8−Lyz, time-dependent H/D exchange in 20, 50, and 100% D_2O for Lyz, Au_n−Lyz, and Cu_n−Lyz (50 and 100%), the mapped surface area of Lyz and Au_8−Lyz, interaction of Lyz with Cu^{2+} and alkali metals, and XPS study of Au_8@Lyz clusters (PDF)

AUTHOR INFORMATION

Corresponding Author

*E-mail: pradeep@iitm.ac.in.

ORCID

Sathish Kumar Mudedla: 0000-0003-3173-5993
Venkatesan Subramanian: 0000-0003-2463-545X
Thalappil Pradeep: 0000-0003-3174-534X

Notes

The authors declare no competing financial interest.

ACKNOWLEDGMENTS

We thank the Department of Science and Technology, Government of India, for continuous support of our research program on nanomaterials. D.G. thanks IIT Madras for student fellowships.

REFERENCES

(1) Xie, J.; Zheng, Y.; Ying, J. Y. Protein-Directed Synthesis of Highly Fluorescent Gold Nanoclusters. *J. Am. Chem. Soc.* **2009**, *131*, 888−889.
(2) Xavier, P. L.; Chaudhari, K.; Baksi, A.; Pradeep, T. Protein-Protected Luminescent Noble Metal Quantum Clusters: An Emerging Trend in Atomic Cluster Nanoscience. *Nano Rev* **2012**, *3*, 14767.
(3) Wei, H.; Wang, Z.; Yang, L.; Tian, S.; Hou, C.; Lu, Y. Lysozyme-Stabilized Gold Fluorescent Cluster: Synthesis and Application as Hg^{2+} Sensor. *Analyst* **2010**, *135*, 1406−1410.
(4) Hu, D.; Sheng, Z.; Gong, P.; Zhang, P.; Cai, L. Highly Selective Fluorescent Sensors for Hg^{2+} Based on Bovine Serum Albumin-Capped Gold Nanoclusters. *Analyst* **2010**, *135*, 1411−1416.
(5) Muhammed, M. A. H.; Verma, P. K.; Pal, S. K.; Retnakumari, A.; Koyakutty, M.; Nair, S.; Pradeep, T. Luminescent Quantum Clusters of Gold in Bulk by Albumin-Induced Core Etching of Nanoparticles: Metal Ion Sensing, Metal-Enhanced Luminescence, and Biolabeling. *Chem.—Eur. J.* **2010**, *16*, 10103−10112.
(6) Wu, X.; He, X.; Wang, K.; Xie, C.; Zhou, B.; Qing, Z. Ultrasmall near-Infrared Gold Nanoclusters for Tumor Fluorescence Imaging in Vivo. *Nanoscale* **2010**, *2*, 2244−2249.

DOI: 10.1021/acs.jpcc.9b04009
J. Phys. Chem. C 2019, 123, 17598−17605

(7) Wang, Y.; Chen, J.; Irudayaraj, J. Nuclear Targeting Dynamics of Gold Nanoclusters for Enhanced Therapy of Her2+ Breast Cancer. *ACS Nano* **2011**, *5*, 9718−9725.
(8) Song, X.-R.; Goswami, N.; Yang, H.-H.; Xie, J. Functionalization of Metal Nanoclusters for Biomedical Applications. *Analyst* **2016**, *141*, 3126−3140.
(9) Chakraborty, I.; Pradeep, T. Atomically Precise Clusters of Noble Metals: Emerging Link between Atoms and Nanoparticles. *Chem. Rev.* **2017**, *117*, 8208−8271.
(10) Desireddy, A.; et al. Ultrastable Silver Nanoparticles. *Nature* **2013**, *501*, 399−402.
(11) Zhu, M.; Aikens, C. M.; Hollander, F. J.; Schatz, G. C.; Jin, R. Correlating the Crystal Structure of a Thiol-Protected Au_{25} Cluster and Optical Properties. *J. Am. Chem. Soc.* **2008**, *130*, 5883−5885.
(12) Krishnadas, K. R.; Ghosh, A.; Baksi, A.; Chakraborty, I.; Natarajan, G.; Pradeep, T. Intercluster Reactions between $Au_{25}(Sr)_{18}$ and $Ag_{44}(Sr)_{30}$. *J. Am. Chem. Soc.* **2016**, *138*, 140−148.
(13) Krishnadas, K. R.; Ghosh, D.; Ghosh, A.; Natarajan, G.; Pradeep, T. Structure-Reactivity Correlations in Metal Atom Substitutions of Monolayer-Protected Noble Metal Alloy Clusters. *J. Phys. Chem. C* **2017**, *121*, 23224−23232.
(14) Krishnadas, K. R.; Baksi, A.; Ghosh, A.; Natarajan, G.; Pradeep, T. Structure-Conserving Spontaneous Transformations between Nanoparticles. *Nat. Commun.* **2016**, *7*, 13447.
(15) AbdulHalim, L. G.; Bootharaju, M. S.; Tang, Q.; Del Gobbo, S.; AbdulHalim, R. G.; Eddaoudi, M.; Jiang, D.-e.; Bakr, O. M. $Ag_{29}(Bdt)_{12}(Tpp)_4$: A Tetravalent Nanocluster. *J. Am. Chem. Soc.* **2015**, *137*, 11970−11975.
(16) Tian, S.; Li, Y.-Z.; Li, M.-B.; Yuan, J.; Yang, J.; Wu, Z.; Jin, R. Structural Isomerism in Gold Nanoparticles Revealed by X-Ray Crystallography. *Nat. Commun.* **2015**, *6*, 8667.
(17) Artymiuk, P. J.; Blake, C. C. F.; Rice, D. W.; Wilson, K. S. The Structures of the Monoclinic and Orthorhombic Forms of Hen Egg-White Lysozyme at 6 Å Resolution. *Acta Crystallogr., Sect. B* **1982**, *38*, 778−783.
(18) Curry, S.; Mandelkow, H.; Brick, P.; Franks, N. Crystal Structure of Human Serum Albumin Complexed with Fatty Acid Reveals an Asymmetric Distribution of Binding Sites. *Nat. Struct. Biol.* **1998**, *5*, 827−835.
(19) Cheng, Y.; Grigorieff, N.; Penczek, P. A.; Walz, T. A Primer to Single-Particle Cryo-Electron Microscopy. *Cell* **2015**, *161*, 438−449.
(20) Cheng, Y. Single-Particle Cryo-Em at Crystallographic Resolution. *Cell* **2015**, *161*, 450−457.
(21) Jadzinsky, P. D.; Calero, G.; Ackerson, C. J.; Bushnell, D. A.; Kornberg, R. D. Structure of a Thiol Monolayer-Protected Gold Nanoparticle at 1.1 Å Resolution. *Science* **2007**, *318*, 430−433.
(22) Chaudhari, K.; Xavier, P. L.; Pradeep, T. Understanding the Evolution of Luminescent Gold Quantum Clusters in Protein Templates. *ACS Nano* **2011**, *5*, 8816−8827.
(23) Chevrier, D. M.; et al. Structure and Formation of Highly Luminescent Protein-Stabilized Gold Clusters. *Chem. Sci.* **2018**, *9*, 2782−2790.
(24) Baksi, A.; Mitra, A.; Mohanty, J. S.; Lee, H.; De, G.; Pradeep, T. Size Evolution of Protein-Protected Gold Clusters in Solution: A Combined Saxs-Ms Investigation. *J. Phys. Chem. C* **2015**, *119*, 2148−2157.
(25) Ghosh, D.; Baksi, A.; Mudedla, S. K.; Nag, A.; Ganayee, M. A.; Subramanian, V.; Pradeep, T. Gold-Induced Unfolding of Lysozyme: Toward the Formation of Luminescent Clusters. *J. Phys. Chem. C* **2017**, *121*, 13335−13344.
(26) Katta, V.; Chait, B. T. Hydrogen/Deuterium Exchange Electrospray Ionization Mass Spectrometry: A Method for Probing Protein Conformational Changes in Solution. *J. Am. Chem. Soc.* **1993**, *115*, 6317−6321.
(27) Baksi, A.; Xavier, P. L.; Chaudhari, K.; Goswami, N.; Pal, S. K.; Pradeep, T. Protein-Encapsulated Gold Cluster Aggregates: The Case of Lysozyme. *Nanoscale* **2013**, *5*, 2009−2016.
(28) Blout, E. R.; De Loze, C.; Asadourian, A. Deuterium Exchange of Water-Soluble Polypeptides and Proteins as Measured by Infrared Spectroscopy. *J. Am. Chem. Soc.* **1961**, *83*, 1895−1900.
(29) Konermann, L.; Pan, J.; Liu, Y.-H. Hydrogen Exchange Mass Spectrometry for Studying Protein Structure and Dynamics. *Chem. Soc. Rev.* **2011**, *40*, 1224−1234.
(30) Liu, C.-L.; et al. Insulin-Directed Synthesis of Fluorescent Gold Nanoclusters: Preservation of Insulin Bioactivity and Versatility in Cell Imaging. *Angew. Chem., Int. Ed.* **2011**, *50*, 7056−7060.
(31) Codreanu, S. G.; Thompson, L. C.; Hachey, D. L.; Dirr, H. W.; Armstrong, R. N. Influence of the Dimer Interface on Glutathione Transferase Structure and Dynamics Revealed by Amide H/D Exchange Mass Spectrometry. *Biochemistry* **2005**, *44*, 10605−10612.
(32) Ghosh, R.; Sahoo, A. K.; Ghosh, S. S.; Paul, A.; Chattopadhyay, A. Blue-Emitting Copper Nanoclusters Synthesized in the Presence of Lysozyme as Candidates for Cell Labeling. *ACS Appl. Mater. Interfaces* **2014**, *6*, 3822−3828.
(33) Goswami, N.; Giri, A.; Bootharaju, M. S.; Xavier, P. L.; Pradeep, T.; Pal, S. K. Copper Quantum Clusters in Protein Matrix: Potential Sensor of Pb^{2+} Ion. *Anal. Chem.* **2011**, *83*, 9676−9680.
(34) Wang, C.; Wang, C.; Xu, L.; Cheng, H.; Lin, Q.; Zhang, C. Protein-Directed Synthesis of Ph-Responsive Red Fluorescent Copper Nanoclusters and Their Applications in Cellular Imaging and Catalysis. *Nanoscale* **2014**, *6*, 1775−1781.
(35) Moreau, S.; Awade, A. C.; Molle, D.; Le Graet, Y. e.; Brule, G. Hen Egg White Lysozyme-Metal Ion Interactions: Investigation by Electrospray Ionization Mass Spectrometry. *J. Agric. Food Chem.* **1995**, *43*, 883−889.
(36) Gokel, G. W.; Barbour, L. J.; Ferdani, R.; Hu, J. Lariat Ether Receptor Systems Show Experimental Evidence for Alkali Metal Cation-Π Interactions. *Acc. Chem. Res.* **2002**, *35*, 878−886.
(37) Gokel, G. W.; De Wall, S. L.; Meadows, E. S. Experimental Evidence for Alkali Metal Cation-Π Interactions. *Eur. J. Org. Chem.* **2000**, 2967−2978.
(38) Wouters, J. Cation-Π (Na^+-Trp) Interactions in the Crystal Structure of Tetragonal Lysozyme. *Protein Sci* **1998**, *7*, 2472−2475.

DOI: 10.1021/acs.jpcc.9b04009
J. Phys. Chem. C 2019, 123, 17598−17605